# Josephson junction with variable thickness of the dielectric layer

T. Dobrowolski and A. Jarmoliński
*Institute of Physics UP, Podchorążych 2, 30-084 Cracow, Poland*

(Received 23 September 2019; revised manuscript received 17 March 2020; accepted 9 April 2020; published 26 May 2020)

The dynamics of the fluxon in the Josephson junction is studied. The dielectric layer of the junction has a variable thickness. It is shown that the modified area of the junction acts on the fluxon as a potential barrier. The relation between the critical bias current and the thickness of the dielectric layer is analytically and numerically determined.

DOI: 10.1103/PhysRevE.101.052215

## I. CONTEXT

At sufficiently low temperatures, some systems, such as the liquids $^3$He and $^4$He, atomic Bose-Einsten condensates, and superconducting materials, exist in coherent states. The issue of the behavior of macroscopic quantum systems has attracted much attention. On the effective level these systems can be described by nonlinear field equations [1]. The properties of these systems have found a variety of technical applications. In particular, superconductors are applied in many devices. For example, two superconductors can be arranged in a device known as a Josephson junction. The state of each superconducting electrode is effectively described by a many-particle wave function. The modulus of this function describes the square root of the density of Cooper pairs in the superconducting material. Because the electrodes are separated by a very thin dielectric layer, the macroscopic wave functions overlap and therefore the only nontrivial variable that describes the dynamics of this system is the gauge-invariant phase difference $\phi$ of the phase factors. This system was first described by Josephson [2] and then this description was confirmed experimentally by Anderson and Rowell [3]. The dynamics of the $\phi$ variable is governed by the sine-Gordon equation [4]. Further modifications of this model, following from the theory of microscopic tunneling, primarily appeared in [5]. This description has been developed up to now [6]. The properties and applications of this model are described in many textbooks and articles [7]. In some physical contexts this equation also appears in a form that explicitly breaks translational invariance [8]. In particular, the Josephson junction is an example of a nonlinear electric circuit, which has attracted the attention of researchers due to its chaotic behavior [9].

The high speeds and low energy dissipation of its switching has motivated the investigation of many electronic devices constructed on the basis of the Josephson junction. The digital electronics based on the flux quanta was proposed in [10]. However, the prospect of rapid single flux quantum (RSFQ) technology based on point junctions is still unclear [11]. Many devices are based on thermal effects in the junction. An example is the topological variant of the superconducting quantum interference proximity transistor (TSQUIPT). This device can act as a thermal switch. Unlike a conventional superconducting quantum interference device (SQUID), this device does not require any ring structure [12]. Another proposal is a very sensitive detector of electromagnetic fields or even a single photon detector based on a SQUID [13]. There are also proposals of superconducting thermal memory devices. Such devices can work even at GHz frequencies [14]. A further, potentially very useful, device can serve as a superconducting thermal router in which the thermal transport can be locally controlled through kink excitations, whose positions can be externally controlled through a bias current or a magnetic field [15]. Other suggestions concern heat engines, energy-harvesting devices, sensing devices, switching devices, and clocking devices for caloritronics circuits and thermal logic [16]. On the other hand, a single topologically protected excitation, which represents a flux quantum, can be pinned by inhomogeneities [17]. Moreover the fluxon can be moved and controlled by bias currents and manipulated through shape engineering [18]. In [19], the curved regions of the junction can act as potential barriers. In this approach, through the appropriate arrangement of the sequence of curved regions, one can prepare the potential barriers. In this context, there is also the idea of the application of two-dimensional junctions with curved boundaries [20]. In this approach, the junction is represented by a flat surface (a surface with zero external curvatures) but curvature effects follow from the curvature of the boundaries of this system. Another proposal concerns the influence of variable width of the junction on the fluxon dynamics [21]. In addition to digital electronics, the Josephson junction can find applications in quantum computing as qubits [22], which are basic elements of quantum computers [23].

In the present paper we study the impact of the varying the thickness of the dielectric layer of the Josephson junction on the kink motion. We expect that the Josephson junction studied by us can potentially be used in high-frequency appliances. In particular, the promising area of applications is technology of superconducting integrated receivers and generators of submillimeter waves [24]. A local variation of the barrier width, including its influence on the fluxon, has been studied before in a number of papers [25]. We consider the influence on the fluxon motion of deforming the regions of the junction. In the next section we formulate the problem.

 

Sections III and IV contain results concerning the interaction of the soliton with a deformed sector of the junction. In these sections we consider the dynamical impact of deforming of the junction on the maximal reflection speed $u_c$ of the fluxon. The results of these sections are used in the description of the sine-Gordon model in the presence of dissipation and the bias current in Secs. V and VI. In these sections we obtain the dependence of the critical bias current on the parameters of the deformation. The critical current separates the situation when the fluxon stops at a deformation from the situation when it passes through it. The last section contains some remarks.

## II. A JUNCTION WITH VARIABLE THICKNESS OF THE DIELECTRIC LAYER

The equation that describes the dynamics of the gauge-invariant phase difference in a long Josephson junction (which is a one-dimensional system) has the form

$$\frac{1}{\bar{c}^2}\,\partial_t^2\phi - \partial_x^2\phi + \frac{1}{\lambda_J^2}\sin\phi = 0, \tag{1}$$

where the Josephson penetration depth $\lambda_J^2 = \frac{h}{2eJ_c\mu_0 d_m}$ is determined by the critical Josephson current $J_c$, Planck's constant $h$, the elementary charge $e$, the permeability of free space $\mu_0$, and the magnetic depth $d_m = 2\lambda_L + a$. The last quantity describes how deeply the magnetic field penetrates the junction. The magnetic depth is specified by the London penetration depths of both superconducting electrodes and the thickness $a$ of the dielectric layer. The variable $x$ specifies the positions of the points along the junction. In the present paper, we consider the impact of varying the thickness of the dielectric layer on the propagation of the fluxons along the junction. In particular we pose the question of whether an area of increased thickness may act as a potential barrier which reflects the fluxon. We assume the dependence of the thickness of the insulator on the space variable of the form $a = a(x) = a_b[1 + \omega(x)]$, where $a_b$ is a basic thickness and the function $\omega(x)$ describes the variation of the thickness from its basic value. In these conditions the total magnetic depth of the junction changes according to the formula $d_m = d_{m0}[1 + \varepsilon\omega(x)]$, where $d_{m0} = 2\lambda_L + a_b$ measures the magnetic depth with respect to the basic thickness of the dielectric layer and $\varepsilon = \frac{a_b}{d_{m0}}$ is a small dimensionless parameter. Under these conditions, the Josephson penetration depth $\lambda_J^2 = \lambda_{J0}^2\frac{1}{1+\varepsilon\omega(x)} = \lambda_{J0}^2\frac{1}{g(x)}$ is a space-dependent quantity, where $\lambda_{J0}^2 = \frac{h}{2eJ_c\mu_0 d_{m0}}$ and the function $g(x) = 1 + \varepsilon\omega(x)$ is related to the thickness by the function $\omega(x)$. Similarly, the Swihart velocity becomes the space-dependent quantity $\bar{c}^2 = c^2\frac{a(x)}{\epsilon_I d_m(x)} = \bar{c}_0^2\frac{1+\omega(x)}{1+\varepsilon\omega(x)} = \bar{c}_0^2\frac{1}{\eta(x)}$; here $\bar{c}_0^2 = c^2\frac{a_b}{\epsilon_I d_{m0}}$ is a constant defined with respect to the basic thickness, $\epsilon_I$ is the permittivity of the insulator that forms the dielectric layer, and $\eta(x) = \frac{1+\varepsilon\omega(x)}{1+\omega(x)}$ is a function that depends on position. In the present paper, we set $\varepsilon = 0.01$. Next, we introduce the dimensionless units $x \to x/\lambda_{J0}$, $t \to t\bar{c}_0/\lambda_{J0}$, and then the field equation for $\phi$ takes the form

$$\eta(x)\partial_t^2\phi - \partial_x^2\phi + g(x)\sin\phi = 0. \tag{2}$$

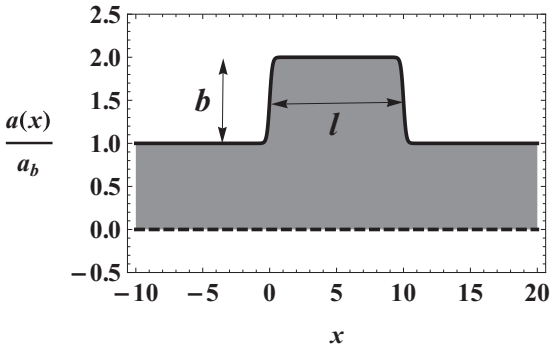


FIG. 1. An example of deformation of the dielectric layer with finite size $l$.

This equation follows from the Lagrangian density

$$\mathcal{L} = \tfrac{1}{2}\eta(x)(\partial_t\phi)^2 - \tfrac{1}{2}(\partial_x\phi)^2 - g(x)(1-\cos\phi). \tag{3}$$

In the subsequent part of this article we consider some particular forms of the function $\omega(x)$. The junctions of this type can be prepared with the use of lithographic techniques. The resolution of these techniques is limited by the wavelength of the source. In this regard, one of the most precise techniques is x-ray and electron lithography, which enables the replication of high-resolution patterns with the use of shadow printing. The simplest arrangement that enables the realization of this technique consists of an electron microscope controlled online by a computer with software enabling the replication of a given pattern [26].

The relative thickness of the dielectric layer, with respect to the basic quantity $a_b$, considered in the present paper is presented in Figs. 1 and 2.

## III. THE MOTION OF THE FLUXON IN THE PRESENCE OF A UNIT STEP DEFORMATION

The Hamiltonian of the system described in the previous section has the form

$$H = \int_{-\infty}^{+\infty} dx\left[\frac{1}{2}\eta(x)(\partial_t\phi)^2 + \frac{1}{2}(\partial_x\phi)^2 + g(x)(1-\cos\phi)\right]. \tag{4}$$

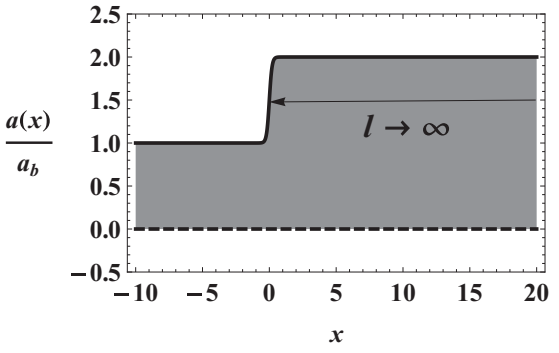


FIG. 2. A deformation of the dielectric layer with unlimited size $l \to \infty$.

The form of the functions $\eta$ and $g$ is crucial for the behavior of the considered system. As a result of numerical simulations, we confirmed that the two models, one described by the functions $\eta(x) = \frac{1+\varepsilon\omega(x)}{1+\omega(x)}$, $g(x) = 1 + \varepsilon\omega(x)$ and the second described by the functions $\eta(x) = \frac{1}{1+\omega(x)}$, $g(x) = 1 + \varepsilon\omega(x)$ for $\varepsilon = 0.01$, produce, with very high accuracy, the same results. In other words, neglecting the linear term with respect to $\varepsilon$ in $\eta$ has no impact on the dynamics of the fluxon. On the other hand, the linear term with respect to small parameter $\varepsilon$ in the case of the function $g(x)$ is crucial for the behavior of the fluxon in the system and therefore cannot be omitted. The neglected linear term in $\eta$ causes only a small local change of the Swihart velocity, whereas a small change of $g(x)$ arranges that there is no reflection from the deformed area. In the further course of this paper we present results for the second system, i.e., the system with neglected linear term (in $\varepsilon$) in the function $\eta$.

The Hamiltonian (4) can be separated into the pure sine-Gordon term and some modifications:

$$H = \int_{-\infty}^{+\infty} dx\left[\frac{1}{2}(\partial_t\phi)^2 + \frac{1}{2}(\partial_x\phi)^2 + (1-\cos\phi)\right] + \int_{-\infty}^{+\infty} dx\left[-\frac{\omega(x)}{2[1+\omega(x)]}(\partial_t\phi)^2 + \varepsilon\omega(x)(1-\cos\phi)\right]. \tag{5}$$

At first, we consider the modifications of the dielectric layer thickness described by the formula $\omega(x) = b[\Theta(x) - \Theta(x-l)]$. In the further parts of this paper, we will show that the behavior of the fluxon is little sensitive to the details of the shape of the function $\omega$. The perturbed part of the Hamiltonian connected with the above deformation can be separated as follows,

$$H = H^{SG} + \int_0^l dx\left[-\frac{b}{2(1+b)}(\partial_t\phi)^2 + \varepsilon b(1-\cos\phi)\right], \tag{6}$$

where $H^{SG}$ represents the pure sine-Gordon Hamiltonian. The Hamiltonian for the fluxon

$$\phi_k(t,x) = 4\arctan[\exp(\xi)], \tag{7}$$

where $\xi = \frac{x-x_0-ut}{\sqrt{1-u^2}}$ is given by the function

$$H = \frac{8}{\sqrt{1-u^2}} + \sqrt{1-u^2}\left[-\frac{4b}{(1+b)}\frac{u^2}{1-u^2} + 4\varepsilon b\right] \times U(l,x_0). \tag{8}$$

Here $U(l,x_0) = \frac{1}{2}[\tanh(\xi_{x=l}) - \tanh(\xi_{x=0})]$. The function $U$ for small velocities is presented in Fig. 3, where $X = x_0 + ut$, and therefore $\xi_{x=l} \approx l - X$ and $\xi_{x=0} \approx -X$. The critical velocity corresponds to the maximum value of the kink speed for which reflection from the deformed area of the junction occurs. In order to calculate this speed, we equate the fluxon energy far from the deformed area (at the beginning of its motion) to the energy of the resting fluxon at the top of the deformation. From (8), at the initial instant $t = 0$, the fluxon is far from the deformed area and therefore $E\,|_{u=u_c,U=0} = \frac{8}{\sqrt{1-u_c^2}}$. At the end of its motion, the fluxon stops at a maximum of

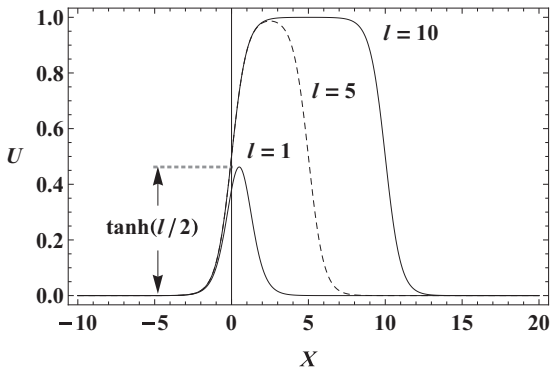


FIG. 3. $U$ as a function of $X$.

$U$ and therefore its energy is $E\,|_{u=0,U\neq 0} = 8 + 4\varepsilon b\tanh(l/2)$. The speed that corresponds to this process is

$$u_c = \sqrt{1 - \frac{1}{\left[1 + \frac{1}{2}\varepsilon b\tanh(l/2)\right]^2}}. \tag{9}$$

The same system could be described in the framework of the perturbational scheme applied to the description of the modified sine-Gordon model in [27]:

$$\partial_t^2\phi - \partial_x^2\phi + \sin\phi = \varepsilon f. \tag{10}$$

In reality, not all of the deformation term present in the Hamiltonian (6) can be considered as a small perturbation. In case of the fluxon (7), we assume a dependence on the variable $\xi = \frac{x-X}{\sqrt{1-u^2}}$, where this time $X = x_0(t) + \int_0^t dt' u(t')$. Approximate equations of motion for $X$ and $u$ are

$$\frac{du}{dt} = -\frac{1}{4}(1-u^2)\int_{-\infty}^{+\infty} dx\,\varepsilon f(\phi(\xi))\,\mathrm{sech}\xi, \tag{11}$$

$$\frac{dX}{dt} = u - \frac{1}{4}u\sqrt{1-u^2}\int_{-\infty}^{+\infty} dx\,\varepsilon f(\phi(\xi))\,\xi\,\mathrm{sech}\xi. \tag{12}$$

Explicit integration leads to the system of ordinary differential equations

$$\frac{du}{dt} = -\frac{1}{4}(1-u^2)^{-3/2}\left(\frac{b}{1+b}\frac{u^2}{1-u^2} + \varepsilon b\right)U_1, \tag{13}$$

$$\frac{dX}{dt} = u - \frac{1}{4}u(1-u^2)\left(\frac{b}{1+b}\frac{u^2}{1-u^2} + \varepsilon b\right)U_2. \tag{14}$$

The auxiliary functions $U_1$ and $U_2$ have the form

$$U_1 = \mathrm{sech}^2\left(\frac{X}{\sqrt{1-u^2}}\right) - \mathrm{sech}^2\left(\frac{l-X}{\sqrt{1-u^2}}\right)$$

and

$$U_2 = -\frac{X}{\sqrt{1-u^2}}\mathrm{sech}^2\left(\frac{X}{\sqrt{1-u^2}}\right) - \frac{l-X}{\sqrt{1-u^2}}\mathrm{sech}^2\left(\frac{l-X}{\sqrt{1-u^2}}\right) + \tanh\left(\frac{X}{\sqrt{1-u^2}}\right) + \tanh\left(\frac{l-X}{\sqrt{1-u^2}}\right).$$

The critical point of the system (13) and (14) corresponds to the fluxon at rest ($u = 0$) at $X = l/2$, the center of the barrier.

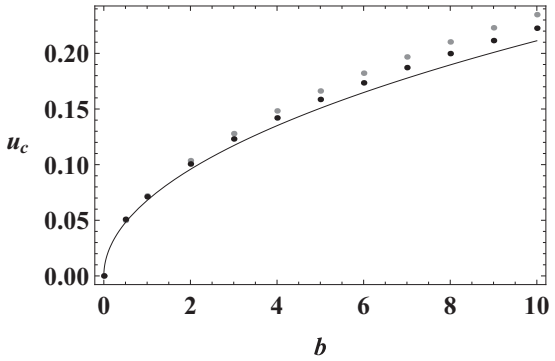


FIG. 4. The critical velocity for $l = 1$. Black points represent numerical results obtained from the field model (2). Gray points represent the results of the simplified dynamical model (13) and (14). The analytical formula is represented by the continuous line.

Now we will compare the values of the critical velocity $u_c$ which follow from the complete field model (2) with those that follow from the approximate dynamical equations (13) and (14) and the analytic formula (9).

The values of the critical speed in Figs. 4 and 5 that follow from the field model are represented by the black points. The values of $u_c$ that follow from the approximate dynamical model are represented by the gray points. The analytical result is represented by the black continuous line. In Fig. 4, which corresponds to a small width of the deformed area $l = 1$, the analytical formula underestimates the numerical values from the field model (2). On the other hand, the approximate dynamical model slightly overestimates the values that follow from the field equation. The situation for larger values of the width of the deformation is different. Figure 5 shows the excellent matching of the analytical formula (9) for $l = 10$ with the numerical result. The approximate dynamical model (13) and (14) significantly overestimates the values of the critical velocities. Moreover we performed numerical simulations for $l \in \{1, 3, 5, 10, 20, 50, 100\}$ and also for $\omega(x) = b\Theta(x)$, which corresponds to an "infinite" width of the deformation. There are two main observations that follow

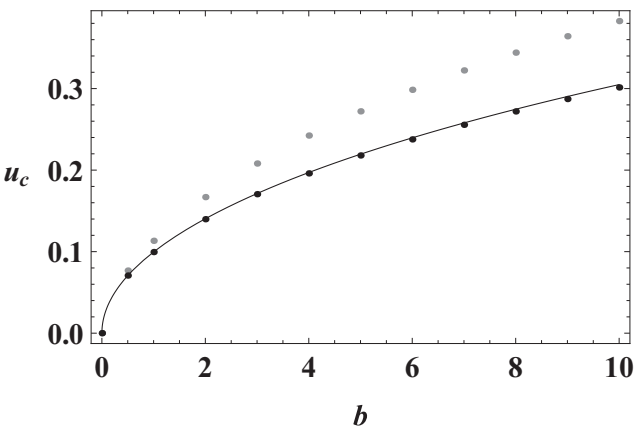


FIG. 5. The critical velocity for $l = 10$. As in the previous figure, black points represent numerical results obtained from the field model. Gray points represent the results of the simplified dynamical model. The analytical formula is represented by the continuous line.

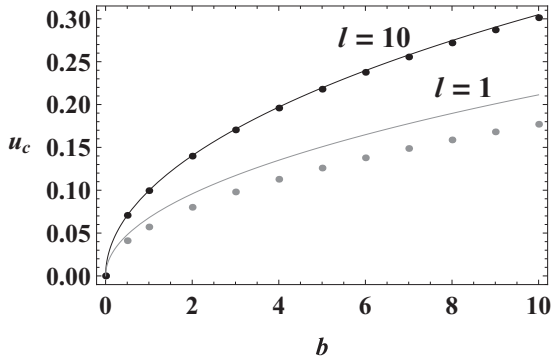


FIG. 6. The critical speed: Comparison of the numerical result of the field model with analytical result for $l = 10$ (black points and line) and $l = 1$ (gray points and line).

from these studies. First, the analytical formula better approximates the numerical results of the field model than does the simplified dynamical model. Second, for $l \geqslant 10$, the precision of the analytical result is similar or identical to the precision presented in Fig. 5. Due to these results, in the further parts of this paper, we will only compare the analytical results with the complete field model.

## IV. INSENSITIVITY OF THE CRITICAL SPEED TO THE DETAILS OF THE SHAPE OF THE DEFORMATION

In this section we test the sensitivity of the formula (9) to the details of the deformation shape. We assume a deformation described by the function $\omega(x) = b\{\tanh(\sigma x) - \tanh[\sigma(x - l)]\}/2$. We performed simulations for different values of the parameters $\sigma$ and $l$. It turns out that the agreement of the numerical analysis with (9) for $\sigma \geqslant 1$ and $l \geqslant 10$ is very good. We performed numerical tests for $l \in \{1, 3, 5, 10, 20, 50, 100\}$ and for the step like function $\omega(x) = b[\tanh(\sigma x) + 1]/2$, which represents an unlimited value of $l$. We also tested different values of the second parameter, namely, $\sigma \in \{0.1, 0.5, 1, 5, 10\}$.

The precision of (9) can be presented with the example of $\sigma = 1$ for $l = 1$ and $l = 10$. In Fig. 6, the numerical data coming from the field model for $l = 1$ are represented by the gray points and the analytical results by the gray continuous line. On the other hand, the corresponding data for $l = 10$ are represented by black points and the black line. At least the same level of precision as for $l = 10$ was obtained whenever $l \geqslant 10$ and simultaneously $\sigma \geqslant 1$. In fact, if the distance $l$ was so large that the function had a clear plato, then the results for small $\sigma$ were also consistent with (9). For instance, such a situation takes place for $\sigma = 0.1$ and $l = 100$.

## V. INFLUENCE OF THE BIAS CURRENT ON THE MOTION OF A KINK WITH A UNIT STEP DEFORMATION

In the previous sections, we considered the ideal system (without dissipation or bias current) in order to extract the impact of the deformed area of the dielectric layer on the fluxon motion. In this section we take into account the dissipation present in real systems and also the presence of the bias current. First for completeness of the presentation we recall

the result that concerns the junction without deformations [27],

$$\partial_t^2\phi + \alpha\,\partial_t\phi - \partial_x^2\phi + \sin\phi = -\gamma. \tag{15}$$

If we multiply both sides of this equation by the time derivative of the $\phi$ and then integrate it with respect to the space variable, we obtain

$$\frac{d}{dt}H^{SG} = -\int_{-\infty}^{+\infty} dx[\gamma\,\partial_t\phi + \alpha\,(\partial_t\phi)^2]. \tag{16}$$

Next, one can put the kink solution (7) into the above formula, thus obtaining an ordinary differential equation for the fluxon velocity

$$\frac{du}{dt} = \frac{1}{4}\,\pi\gamma(1-u^2)^{\frac{3}{2}} - \alpha\,u(1-u^2). \tag{17}$$

The constant equilibrium solution of this equation, $u_s =$ constant, corresponds to the situation when the loss of power due to dissipation is balanced by the power input caused by the bias current:

$$u_s = \frac{1}{\sqrt{1+\left(\frac{4\alpha}{\pi\gamma}\right)^2}}. \tag{18}$$

This speed corresponds to stationary motion of the fluxon in the junction. Equipped with this knowledge, we can consider the system which is the main subject of the present paper: a junction with a locally deformed dielectric layer. This system is described by the equation

$$\eta(x)\,\partial_t^2\phi + \alpha\,\partial_t\phi - \partial_x^2\phi + g(x)\sin\phi = -\gamma. \tag{19}$$

In this section, as in Sec. III, the deformation is described by the function $\omega(x) = b[\Theta(x) - \Theta(x-l)]$. The formula (18) relates the bias current with the velocity which corresponds to stationary motion (in our case far from the deformation). If the velocity of the fluxon $u_s$ does not exceed the critical value (9), then the fluxon stops at the position of the deformation. In the opposite case, the fluxon passes through the deformation. The critical value of the bias current $\gamma_c$ that separates these two regimes corresponds to $u_s = u_c$, i.e.,

$$\gamma_c = \frac{4}{\pi}\,\alpha\sqrt{\frac{u_c^2}{1-u_c^2}}, \tag{20}$$

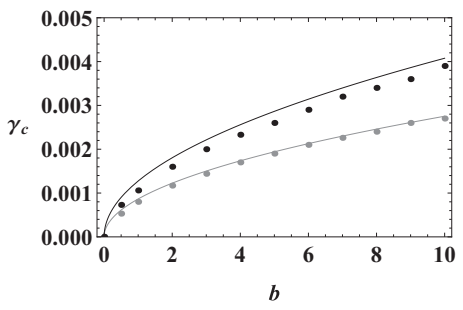


FIG. 7. The critical value of the bias current as a function of the thickness of the dielectric layer. The numerical results (gray points) compared with those of the analytical formula (20) (gray line) for $l = 1$. For $l = 10$, black points (numerical) and black line (analytical).

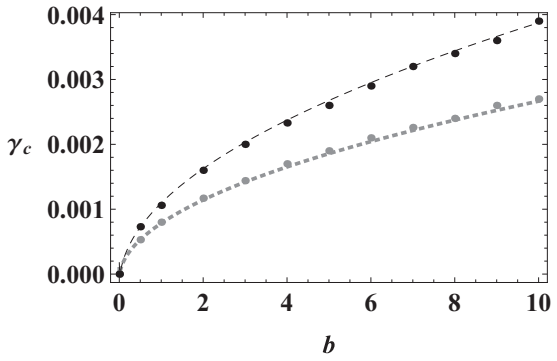


FIG. 8. The critical value of bias current as a function of the thickness parameter $b$. The corrected analytical formula (21) is compared with the numerical values. Black dashed line and black points correspond to $l = 10$. Gray dotted line and gray points describe the case of $l = 1$.

where the critical speed $u_c$ is given by (9). A graphical comparison of the numerical results of the field model (19) with those of (20) is presented in Fig. 7. The gray continuous line and gray points represent the analytical results and the numerical simulations for $l = 1$. The analytical formula in this case fits the numerical data very well. The black continuous line and black points represent the analytical result and the numerical data for $l = 10$. This time we observe some discrepancy between the analytical result and the numerical data. Moreover, we observe the same level of discrepancy for $l \geqslant 10$, i.e., for $l = 10, 20, 50, 100$. In order to improve the consistency of the results we introduced into the formula (20) an empirical correction of the critical speed,

$$\gamma_c = \frac{4}{\pi}\,\alpha\sqrt{\frac{(u_c-\Delta u_c)^2}{1-(u_c-\Delta u_c)^2}}, \tag{21}$$

where $\Delta u_c = u_0\tanh(l/2)$ and the factor $u_0$ is fitted for all values of $l$ by $u_0 = 0.0138$. The corrected formula (21) is compared with the numerical results in Figs. 8 and 9 for different ranges of $b$. The gray dotted line corresponds to $l = 1$ and the black dashed to $l = 10$. A similar level of agreement is reached for all other values of $l$.

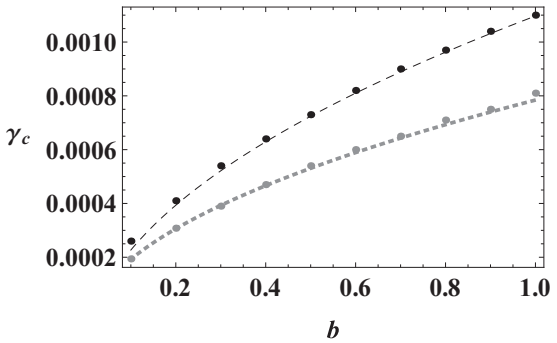


FIG. 9. The numerical values of the critical bias current compared with the modified analytical formula (21). Black dashed line and black points correspond to $l = 10$. Gray dotted line and gray points describe the case of $l = 1$. The results concern a narrower range of the thickness parameter $b$ than in Fig. 8.

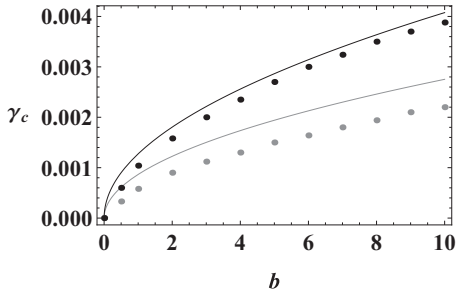


FIG. 10. Critical values of bias current for $l = 10$ black continuous line compared with black dots and for $l = 1$ gray continuous line compared with gray dots. Dots represent numerical values of the field model and the continuous lines represent analytical result. In all cases $\sigma$ is set equal to 1.

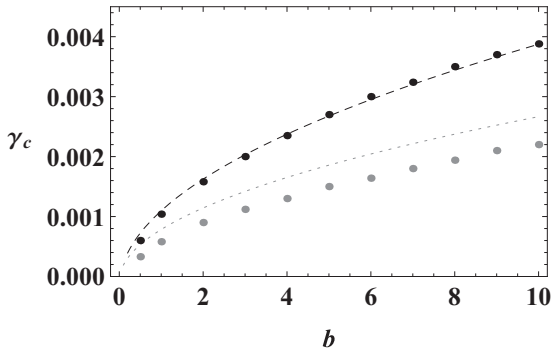


FIG. 11. The improved analytical formula (21) compared with numerical results from the field model. The black, respectively, gray points represent the numerical results for $l = 10$, respectively, $l = 1$. The improved analytical formula is represented by the dashed black line for $l = 10$ and gray dotted line for $l = 1$.

## VI. LIMITS OF INSENSITIVITY OF THE CRITICAL BIAS CURRENT TO THE DETAILS OF THE SHAPE OF THE DEFORMATION

In order to test how much the analytical results of the previous section are sensitive to the details of the deformation, we once again consider the system defined by Eq. (19), but this time we consider a deformation of the form $\omega(x) = b\{\tanh(\sigma x) - \tanh[\sigma(x - l)]\}/2$. First we compare the behavior of the system that follows from the field model with the predictions of (20). In Fig. 10, the numerical values of the critical bias current for the small width of the deformation $l = 1$ are represented by gray points and the values that follow from the analytical formula (20) are represented by the gray line. Similarly, the numerical values of the field model for $l = 10$ are represented by black points and the black continuous line represents the analytical result for this deformation width. In Fig. 10, the second parameter is set to $\sigma = 1$. In both cases, (20) overestimates the numerical values. Moreover, the relative error of this formula for $l = 1$ is significantly greater than the error for $l = 10$. We also performed a comparison for different values of $l$ and $\sigma$ and we noticed that for $l \geqslant 10$ and $\sigma \geqslant 1$, the error is similar to that in the case $l = 10$ and $\sigma = 1$. A similar comparison is presented for the case of the corrected formula (21). This time, the analytical formula for $l = 1$ is represented by the dotted gray line and the formula for $l = 10$ is represented by the dashed black line. For $l = 10$ we observe a very good compatibility of the corrected analytical formula (21) with the field model predictions, while for $l = 1$, (21) overestimates the numerical values. In both cases, in the figure the second parameter is set to $\sigma = 1$. Moreover, we compare the numerical values from the field model with the results of the improved formula (21) and have a similar consistency (as for $l = 10$ in Fig. 11) for all $l \geqslant 10$ and $\sigma \geqslant 1$.

## VII. REMARKS

What is crucial for potential applications of the described system is the fact that regions with an increased thickness of the dielectric layer act on the fluxon as a potential barrier. We have shown that the details of the deformation of the dielectric layer have a negligible impact on the fluxon dynamics. This allows forming potential barriers that can be used for the storage of fluxons. We have proposed a formula that relates the value of the critical bias current with the essential parameters of the shape of the deformation. Summing up, we have proposed an analytical description of Josephson junctions with variable thickness of the dielectric layer. In these junctions, properly prepared dielectric layers make it possible to store fluxons on one side of a potential barrier. The crucial condition for the transition of a fluxon through such a barrier is the value of the applied bias current. Whenever the bias current exceeds the critical value, we observe the transmission of the fluxon. In the opposite case, the fluxon is stored on one side of the deformed area.

One of the possible applications of the described junction could be the generation of high-frequency submillimeter waves. This technology is justified by the development of practical systems [24].

[1] M. J. Ablowitz and P. A. Clarkson, *Solitons, Nonlinear Evolution Equations, and Inverse Scattering* (Cambridge University Press, Cambridge, 1999); N. F. Pederson, in *Solitons*, edited by S. E. Trullinger, V. E. Zakharov, and V. L. Pokrovsky, (Elsevier, Amsterdam, 1986), pp. 469–502; L. A. Ferreira, B. Piette, and W. J. Zakrzewski, Phys. Rev. E **77**, 036613 (2008); J. Phys. C **128**, 012027 (2008); V. G. Ivancevic and T. T. Ivancevic, J. Geom. Symmetry Phys. **31**, 1 (2013); C. Adam, M. Haberichter, and A. Wereszczynski, Phys. Lett. B **754**, 18 (2016).

[2] B. D. Josephson, Phys. Lett. **1**, 251 (1962).

[3] P. W. Anderson and J. M. Rowell, Phys. Rev. Lett. **10**, 230 (1963).

[4] B. D. Josephson, Adv. Phys. **14**, 419 (1965).

[5] N. R. Werthamer, Phys. Rev. **147**, 255 (1966); A. I. Larkin and Yu. N. Ovchinnikov, Sov. Phys. JETP **24**, 1035 (1967) [**51**, 1535 (1966)].

[6] D. R. Gulevich, V. P. Koshelets, and F. V. Kusmartsev, Phys. Rev. B **96**, 024515 (2017); D. R. Gulevich, L. V. Filippenko, and V. P. Koshelets, J. Low Temp. Phys. **194**, 312 (2019);

D. R. Gulevich, V. P. Koshelets, and F. V. Kusmartsev, Phys. Rev. B **99**, 060501(R) (2019); D. R. Gulevich, Comput. Phys. Commun. **251**, 107091 (2020).

[7] A. R. Bishop and T. Schneider, *Solitons and Condensed Matter Physics* (Springer, Berlin, 1981); A. S. Davydov, *Solitons in Molecular Systems* (Reidel, Dordrecht, 1985); A. Barone and G. Paterno, *Physics and Applications of the Josephson Effect* (Wiley, New York, 1982); A. Barone, F. Esposito, C. J. Magee, and A. C. Scott, Riv. Nuovo Cimento **1**, 227 (1971); J. D. Gibbon, I. N. James, and I. M. Moroz, Phys. Scr. **20**, 402 (1979); S. V. Kuplevakhsky and A. M. Glukhov, Phys. Rev. B **73**, 024513 (2006); **76**, 174515 (2007).

[8] C. Adam, K. Oles, T. Romanczukiewicz, and A. Wereszczynski, arXiv:1902.07227; C. Adam and A. Wereszczynski, Phys. Rev. D **98**, 116001 (2018).

[9] F. Li, Q. R. Liu, H. Y. Guo, Y. H. Zhao, J. Tang, and J. Ma, Nonlinear Dyn. **69**, 2169 (2012); T. Kawaguchi, Phys. C: Superconduct. Applic. **471**, 824 (2011); A. E. Botha, Y. M. Shukrinov, and M. R. Kolahchi, Chaos, Solitons & Fractals **48**, 32 (2013); M. A. Ferré, M. G. Clerc, S. Coulibally *et al.*, Eur. Phys. J. D **71**, 172 (2017); Z. Yao, J. Ma, Y. Yao, and C. Wang, Nonlinear Dyn. **96**, 205 (2019); R. H. Goodman, Chaos **18**, 023113 (2008).

[10] T. A. Fulton, R. C. Dynes, and P. W. Anderson, Proc. IEEE **61**, 28 (1973); M. Cirillo, J. Appl. Phys. **58**, 3217 (1985); K. K. Likharev, O. A. Mukhanov, and V. K. Semenov, in *SQUID'85: Superconducting Quantum Interferences Devices and Their Applications* (de Gruyter, Berlin, 1985), p. 1103; J. Ren and V. K. Semenov, IEEE Trans. Appl. Supercond. **21**, 780 (2011).

[11] K. Likharev, Phys. C (Amsterdam) **482**, 6 (2012).

[12] L. Bours, B. Sothmann, M. Carrega, E. Strambini, E. M. Hankiewicz, L. W. Molenkamp, and F. Giazotto, Phys. Rev. Appl. **10**, 014027 (2018).

[13] T. T. Heikkilä, R. Ojajärvi, I. J. Maasilta, E. Strambini, F. Giazotto, and F. S. Bergeret, Phys. Rev. Appl. **10**, 034053 (2018); P. Solinas, F. Giazotto, and G. P. Pepe, *ibid.* **10**, 024015 (2018).

[14] C. Guarcello, P. Solinas, A. Braggio, M. Di Ventra, and F. Giazotto, Phys. Rev. Appl. **9**, 014021 (2018); C. Guarcello, P. Solinas, M. Di Ventra, and F. Giazotto, *ibid.* **7**, 044021 (2017); C. Guarcello, F. Giazotto, and P. Solinas, Phys. Rev. B **94**, 054522 (2016); C. Guarcello, P. Solinas, M. Di Ventra, and F. Giazotto, Sci. Rep. **7**, 46736 (2017).

[15] C. Guarcello, P. Solinas, A. Braggio, and F. Giazotto, Phys. Rev. Appl. **9**, 034014 (2018).

[16] C. Guarcello, P. Solinas, A. Braggio, and F. Giazotto, Sci. Rep. **8**, 12287 (2018); G. De Simoni, F. Paolucci, P. Solinas, E. Strambini, and F. Giazotto, Nat. Nanotechnol. **13**, 802 (2018).

[17] A. V. Ustinov, in *Nonlinear Superconductive Electronics and Josephson Devices*, edited by G. Costabile, S. Pagano, N. F. Pedersen, and M. Russo (Springer US, Boston, 1991), pp. 315–336; R. Fehrenbacher, V. B. Geshkenbein, and G. Blatter, Phys. Rev. B **45**, 5450 (1992).

[18] K. Nakajima *et al.*, J. Appl. Phys. **47**, 1620 (1976); A. Benabdallah, J. G. Caputo, and A. C. Scott, Phys. Rev. B **54**, 16139 (1996); A. Kemp, A. Wallraff, and A. V. Ustinov, Phys. Status Solidi B **233**, 472 (2002); Phys. C (Amsterdam) **368**, 324 (2002); D. R. Gulevich and F. V. Kusmartsev, Phys. Rev. Lett. **97**, 017004 (2006); New J. Phys. **9**, 59 (2007); D. R. Gulevich, M. Gaifullin, O. E. Kusmartseva, F. V. Kusmartsev, and K. Hirata, Phys. C (Amsterdam) **468**, 1903 (2008); D. R. Gulevich, F. V. Kusmartsev, S. Savel'ev, V. A. Yampol'skii, and F. Nori, Phys. Rev. Lett. **101**, 127002 (2008); J.-G. Caputo and D. Dutykh, Phys. Rev. E **90**, 022912 (2014); R. Monaco, J. Phys.: Condens. Matter **28**, 445702 (2016); R. Monaco *et al.*, Supercond. Sci. Technol. **31**, 025003 (2018).

[19] T. Dobrowolski, Phys. Rev. E **79**, 046601 (2009); Eur. Phys. J. B **86**, 346 (2013); in *Geometry, Integrability, and Quantization*, edited by I. M. Mladenov, G. Meng, and A. Yoshioka (Avangard Prima, Sofia, 2016), pp. 182–195; A. Jarmoliński and T. Dobrowolski, Phys. B: Condensed Matter **514**, 24 (2017); T. Dobrowolski and A. Jarmoliński, Phys. Rev. E **96**, 012214 (2017); Results Phys. **8**, 48 (2018).

[20] C. Gorria, Yu. B. Gaididei, M. P. Soerensen, P. L. Christiansen, and J. G. Caputo, Phys. Rev. B **69**, 134506 (2004); E. Goldobin, A. Sterck, and D. Koelle, Phys. Rev. E **63**, 031111 (2001); G. Carapella, G. Costabile, N. Martucciello, M. Cirillo, R. Latempa, A. Polcari, and G. Filatrella, Phys. C (Amsterdam) **382**, 337 (2002); G. Carapella, N. Martucciello, and G. Costabile, Phys. Rev. B **66**, 134531 (2002); D. R. Gulevich and F. V. Kusmartsev, Supercond. Sci. Technol. **20**, S60 (2007).

[21] Yu. Koval, A. Wallraff, M. Fistul, N. Thyssen, H. Kohlstedt, and A. V. Ustinov, IEEE Trans. Appl. Supercond. **9**, 3957 (1999).

[22] S. Han, Y. Yu, Xi Chu, S. Chu, and Z. Wang, Science **293**, 1457 (2001); Y. Nakamura, Y. A. Pashkin, T. Yamamoto, and J. S. Tsai, Phys. Rev. Lett. **88**, 047901 (2002); D. Vion, A. Aassime, A. Cottet, P. Joyez, H. Pothier, C. Urbina, D. Esteve, and M. H. Devoret, Science **296**, 886 (2002); J. M. Martinis, S. Nam, J. Aumentado, and C. Urbina, Phys. Rev. Lett. **89**, 117901 (2002); Y. Yu, S. Han, X. Chu, S. Chu, and Z. Wang, Science **296**, 889 (2002); A. J. Berkley, H. Xu, R. C. Ramos, M. A. Gubrud, F. W. Strauch, P. R. Johnson, J. R. Anderson, A. J. Dragt, C. J. Lobb, and F. C. Wellstood, *ibid.* **300**, 1548 (2003); I. Chiorescu, Y. Nakamura, C. J. P. M. Harmans, and J. E. Mooij, *ibid.* **299**, 1869 (2003); Yu. A. Pashkin, T. Yamamoto, O. Astafiev, Y. Nakamura, D. V. Averin, and J. S. Tsai, Nature (London) **421**, 823 (2003).

[23] M. A. Nielsen and I. L. Chuang, *Quantum Computation and Quantum Information* (Cambridge University Press, Cambridge, 2000).

[24] V. P. Koshelets and S. V. Shitov, Supercond. Sci. Technol. **13**, R53 (2000); V. P. Koshelets, S. V. Shitov, L. V. Filippenko, A. M. Baryshev, W. Luinge, H. Golstein, H. van de Stadt, J.-R. Gao, and T. de Graauw, IEEE Trans. Appl. Supercond. **7**, 3589 (1997); G. de Lange *et al.*, Supercond. Sci. Technol. **23**, 045016 (2010); O. Kiselev, M. Birk, A. Ermakov, L. Filippenko, H. Golstein, R. Hoogeveen, N. Kinev, B. van Kuik, A. de Lange, G. de Lange, P. Yagoubov, and V. Koshelets, IEEE Trans. Appl. Supercond. **21**, 612 (2011).

[25] A. Shnirman, E. Ben-Jacob, and B. Malomed, Phys. Rev. B **56**, 14677 (1997); P. D. Shaju and V. C. Kuriakose, Phys. Lett. A **332**, 326 (2004); A. N. Price, A. Kemp, D. R. Gulevich, F. V. Kusmartsev, and A. V. Ustinov, Phys. Rev. B **81**, 014506 (2010).

[26] A. N. Broers, IBM J. Res. Dev. **32**, 502 (1988); X. Du, I. Skachko, and E. Y. Andrei, Phys. Rev. B **77**, 184507 (2008).

[27] D. W. McLaughlin and A. C. Scott, Phys. Rev. A **18**, 1652 (1978).